

Differential gene expression in *Bacillus subtilis*

Dagmar Iber¹, Joanna Clarkson², Michael D. Yudkin², Iain D. Campbell³

¹Mathematical Institute, Centre for Mathematical Biology, University of Oxford, 24-29 St Giles
Oxford OX1 3LB, UK; E-mail: iber@maths.ox.ac.uk

²Microbiology Unit, ^{2,3}Department of Biochemistry, University of Oxford, South Parks Road,
OX1 3QU, Oxford, UK

Sporulation in *Bacillus subtilis* serves as a paradigm for the development of two different cell types (mother cell and prespore) from a single cell. The mechanism by which the two different developmental programs are initiated has been much studied but is not well understood. With the help of existing and new experimental results, a mathematical model has been developed that reproduces all published *in vitro* experiments and makes new predictions about the properties of the system *in vivo*.

Introduction

Multicellular organisms achieve cell differentiation by selective expression of genes but the mechanisms that trigger such differential expression are difficult to define. Single-celled prokaryotes offer several experimental advantages for studies of cell differentiation; a good example is spore formation in *Bacillus subtilis* which is induced by nutritional stress. During sporulation the single cell organism differentiates into two cell types, a smaller forespore (prespore) and a larger mother cell, separated by a septum. The two different developmental programs are initiated by the transcription factor σ^F , which associates with the core RNA polymerase in the prespore but not in the mother cell. In the mother cell σ^F is trapped in a complex with SpoIIAB (hereafter referred to as AB). While the pathways that lead to σ^F dissociation are well-defined, it is not yet clear why σ^F association with the core RNA polymerase is restricted to the prespore [1].

Crystallography has demonstrated that one molecule of σ^F binds asymmetrically across the two subunits of the AB dimer [2]. The binding of σ^F prevents access of SpoIIAA (hereafter referred to as AA) to one monomer of AB, but allows docking of AA on the other monomer [3]. Steric and electrostatic clashes are caused by the docking of AA, and σ^F is subsequently displaced from AB [4, 3]. AA binds across the nucleotide-binding pocket of AB, and is phosphorylated when this binding pocket contains ATP, yielding inactive phosphorylated AA (AA-P) and AB·ADP. AB·ADP can either be sequestered in an AA·AB·ADP complex or exchange ADP for ATP. Free AB (in both its ATP and ADP forms) can rebind σ^F , and sustained σ^F release is thus expected to require reactivation of AA-P by SpoIIE-mediated dephosphorylation [5].

The restriction of σ^F release to the prespore has been ascribed to two aspects of asymmetric septation: i) the volume difference between prespore and mother cell, together with the accumulation of SpoIIE (hereafter referred to as IIE) on the septum [6]; ii) loss of AB in the prespore, caused by a transient genetic imbalance, as described below [7, 8]. Accumulation of IIE on (both sides of) the septum results in an increase in IIE activity in the smaller prespore and reduced activity in the larger mother cell. It has been suggested that the increase in IIE activity may lead to sufficient dephosphorylation of AA-P to trigger σ^F release specifically in the forespore [6], and recent biochemical experiments indeed reveal that σ^F ·AB complexes are highly sensitive to small changes in IIE activity [9]. The resulting release of σ^F in the prespore might be reinforced by rapid degradation of unbound AB [10, 8], which would prevent reassociation of σ^F and AB. Degradation of AB is not balanced by protein expression in the prespore because of a transient genetic imbalance; this arises from the fact that about 70% of the chromosome (including the *spoIIA* operon in which AB is coded) is initially excluded from the forespore and is imported into it only 10-20 minutes after septum closure [11]. A further proposed result of the genetic imbalance is the degradation and loss of a IIE inhibitor from the prespore, which would further accelerate σ^F release [7]. The nature of such an inhibitor is, however, still elusive, and while the concentration of IIE on the septum and the degradation of AB in the forespore have both been shown to be important for successful sporulation, interference with either one of them does not abolish sporulation [8, 12]. No model yet explains how these small and transient differences act together to maintain the release of σ^F for at least 1h. Moreover, it is unclear whether these processes are sufficient for the initiation of sporulation or whether other, still unidentified, factors play a role [1].

By employing a combination of experimental and mathematical modeling tools we derive the regulatory circuit that controls σ^F release. A large amount of information is available about the properties of this system, and most of the kinetic and thermodynamic parameters

are known. Our model quantitatively reproduces the system's known behaviour *in vitro*, including the sensitivity of AB- σ^F complexes to small changes in IIE activity and in AA concentration. The model predicts that SpoIIE relocation to the septum is sufficient for prespore-specific formation of σ^F -RNA polymerase holoenzyme and that the required sensitivity stems from SpoIIAB allostery, which we confirm experimentally. Stochastic fluctuations in gene expression are buffered by coupled translation of SpoIIAA and SpoIIAB combined with degradation of unbound SpoIIAB, while ATP consumption is limited by the formation of SpoIIAA-SpoIIAB-ADP. The transient genetic imbalance plays no important role.

Construction of the mathematical model

The pathway that controls σ^F release

The key steps and players involved in the regulation of σ^F can be summarized as follows. σ^F binds asymmetrically across the two subunits of the AB dimer [2] and is displaced by steric and electrostatic clashes that are caused by the docking of SpoIIAA (AA) [4, 3]. AA binds across the nucleotide-binding pocket of AB, and is phosphorylated when this binding pocket contains ATP, yielding inactive phosphorylated AA (AA-P) and AB-ADP. AB-ADP can either be sequestered in an AA-AB-ADP complex or exchange ADP for ATP. Free AB (in both its ATP and ADP forms) can rebind σ^F , and sustained σ^F release is thus expected to require reactivation of AA-P by SpoIIE-mediated dephosphorylation [5].

A model for the pathway that controls σ^F release

During early attempts to develop a model of the system described in Figure 1A in the main paper it became clear that some extensions would be necessary. One important extension, confirmed by new experiments is that AB, which is a dimer, binds AA with positive cooperativity (see below). This cooperative behaviour increases the number of reactions that need to be considered in the model. The shaded part of the scheme summarizes the interactions of one AB conformer and therefore includes only the well-known reactions that have been reviewed extensively (see Hilbert and Piggot (2004) and references therein). In brief, binding of σ^F to AB-ATP (61/62 - all following numbers in round brackets refer to reactions in our model) leads to the formation of a σ^F -AB-ATP complex [13]. σ^F in this complex cannot bind to core RNA polymerase and is thus termed inactive [13, 14]. Subsequent interaction with AA leads to the formation of σ^F -AB-ATP-AA (43/44), from which σ^F is rapidly released (79/80) [15]. Consistent with structural information derived from crystallography [2, 4], binding of two AA to the AB dimer while σ^F is still bound is impossible [3]. The bound AA can be phosphorylated either immediately (185) or after a further AA has bound (189) [14]. AA-P can be reactivated by the phosphatase action of IIE (193-195; [6, 16]). AB-ADP can either bind AA (9-12, 35/36, 158) or rebinding σ^F - either immediately (63/64) or after ADP-ATP exchange (140-143, 170-173) [5]. ADP-ATP exchange is also possible when AA is bound to AB-ADP (162, 164) and dimers with no, or two different, nucleotides bound (19-26, 53-56, 69/70, 86/87, 92/93, 156/157, 178/179, 186, 191) also need to be considered.

Given the allosteric behaviour of AB the scheme had to be extended to include also a second AB conformer (non-shaded part) as well as interconversions between AB states (94-137). This leads to a duplication of almost all the interactions mentioned so far. Only in the case of AA

and σ^F binding to nucleotide-free AB could the unfavoured conformation be neglected, since a comparison of the relevant parameters shows that these interactions would be of significance neither in the *in vitro* experiments nor in the sporulating cell. In the diagram, the conformation that binds AA with low affinity and ADP with higher affinity is depicted as circles (AB), and the other state as squares (\hat{AB}). As is usual for descriptions of allosteric proteins (e.g. [17]) these two states may be referred to as the tense (T) and the relaxed (R) state respectively.

SpoIIAB is an allosteric protein

Our experiments with fluorescence quenching, a Scatchard plot, and surface plasmon resonance (SPR) all provide evidence for the allosteric behaviour of SpoIIAB. The non-cooperative binding mechanism of published models failed to fit results from fluorescence quenching data obtained with AA and AB-F97W, a fluorescent derivative of AB [18]. When AB-F97W was mixed with AA, less than an equimolar AA concentration was needed to quench half the fluorescence (Fig. 1 A). The effect was even stronger with the lower affinity AA mutant, AA-S58A, suggesting that binding of one AA to AB induces a conformational change which results in quenching of the fluorescence on the second non-bound monomer. A Scatchard analysis confirmed the allosteric behaviour of AB (see Fig. 2A in the main paper). The experiments had to be carried out with the AA-S58A mutant to avoid AA phosphorylation by trace amounts of ATP. (The AA/AB ratio is apparently overestimated by a factor of about 1.3, presumably because of errors in the determination of protein concentrations, and these probably explain the $\nu > 2$ result). Moreover, SPR binding kinetics obtained with AB bound to the sensor chip are better fitted by an allosteric model (see below). Consistent with the hypothesis that AB is an allosteric protein, crystallographic structures of AB in complex with either σ^F or AA [2, 4] have shown it to be a flexible molecule. The conformation of AB is sensitive to the type of ligand bound, with changes occurring within the nucleotide-binding region and in the angle between the subunits. However, our model assumes that both the σ^F - and AA-bound forms of AB are predominantly in the R-state, with the result that changes between the states would not be visible in the crystal structures because of low occupancy of the T state.

Parameter determination

Lack of quantitative data and experimental detail have often restricted the predictive power of mathematical models. This study has greatly benefited from the large amount of published experimental information and the availability of a well-established *in vitro* system. Values for essentially all the key parameters could thus be determined experimentally. The almost 200 rate constants included in the scheme were reduced to 30 independent rate constants by assuming that the kinetic constants of one AB monomer are not affected by ADP, ATP or AA being bound to the other monomer other than through a change in the relative concentration of the R and T states.

The 27 independent kinetic constants for the *in vitro* model can be grouped into those characterising the AB-AA interaction (reactions 1-58), the AB- σ^F interaction in the absence (59-76) or presence (77-93) of AA, the interconversion between the R and the T state (94-137), the ADP-ATP exchange (138-182), and finally the phosphorylation (183-192) and dephosphorylation (193-195) of AA. The values of many of these parameters have already been published. However, most of the on- and off-rates have been determined by SPR; this technique requires the proteins analysed to be attached to a sensor chip, which may alter their behavior. Fluorescence quenching experiments do not have this shortcoming, and a re-analysis of important

kinetic parameters was carried out by fluorescence spectroscopy with the help of fluorescent mutants [18, 15]. Constants that had been determined on the assumption that AB is not an allosteric protein were refined to fit the model.

AB-AA binding constants

The first group of constants are those characterising the AB-AA interaction (1-58). The rate constants for the formation of the AB·AA complex in the presence of ADP can be determined by SPR following the protocol established by Magnin *et al* (1997). These measurements can be carried out with either AB or AA bound to the sensor chip. However, AA-interactions with both AB monomers will occur only when AB is bound to the chip, since the spacing of chip-bound AA is unlikely to be appropriate for AB to bind to two molecules of AA. For the monomeric interaction when AA is chip-bound a total of 15 experiments were pooled from Shu *et al* (2004) together with other unpublished results from this laboratory. The on- and off-rates were determined as $k_{on}^* = 1.6 \times 10^5 \text{ M}^{-1}\text{s}^{-1}$ ($\pm 2.1 \times 10^5$ standard deviation) and $k_{off}^* = 6.85 \times 10^{-3} \text{ s}^{-1}$ ($\pm 4 \times 10^{-3}$ standard deviation) respectively. Here the off-rate will correspond to the the high affinity state, since upon binding of AA, AB will undergo a conformational change to the high affinity form.

To facilitate the fitting of the binding of two AA molecules to one chip-bound AB molecule by means of the Biacore software we exploited the fact that one conformation of the AB and AB·AA₂ dimers is particularly favored; we thus simplified the binding reaction to a 3-step mechanism involving an initial binding of one AA to the AB dimer (in the low affinity state), a subsequent conformational switch and the binding of a second AA to AB·AA in the high affinity state. Fitting of SPR data with this 3-step mechanism was substantially improved over that with a single step (non-allosteric) model, with the average χ^2 value of the fit being reduced by approximately 10-fold. (In contrast fitting was not improved by the 3-step mechanism when AA was bound to the chip.) The estimates obtained from 5 unpublished experiments for the on- and off-rates of the two binding steps were $k_{on1} = 1.1 \times 10^6 \text{ M}^{-1}\text{s}^{-1}$ ($\pm 10^6$ standard deviation), $k_{on2} = 4 \times 10^4 \text{ M}^{-1}\text{s}^{-1}$ ($\pm 2.9 \times 10^4$ standard deviation), $k_{off1} = 2.4 \text{ s}^{-1}$ (± 2.2 standard deviation), $k_{off2} = 8.4 \times 10^{-3} \text{ s}^{-1}$ ($\pm 1.7 \times 10^{-3}$ standard deviation). The conformational change occurs at 7.4 s^{-1} (± 5.6 standard deviation) and 2 s^{-1} (± 1 standard deviation) towards the high and low affinity states respectively. The affinity of the second bound AA will probably have been underestimated by SPR since attachment of AB to the grid is likely to obscure at least one binding site and to constrain conformational changes. Equally the AA-AB on-rate will have been underestimated when AA is fixed to the grid since AA, the smaller protein, will diffuse more rapidly when both are in solution. We therefore used an intermediate value $k_{on1} = 8 \times 10^5 \text{ M}^{-1}\text{s}^{-1}$ as the general AA-AB on-rate in our simulations, and $7.4 \times 10^{-3} \text{ s}^{-1}$ as the off-rate in the high affinity state, which is the average value of all measurements made. k_{off1} and the rate for the conformational change in the disfavoured direction were used as determined by SPR above. In order to fit AA-AB binding as measured in fluorescence quenching experiments (Fig. 1) the conformational change towards the favoured state had to be taken to be higher than estimated by SPR. We used 20 s^{-1} ; a higher value would further improve the fit in Figure 1a. A likely explanation for the lower value for the SPR measurement is that fixation to the chip impairs AB conformational changes.

The binding constants in the presence of ATP are more difficult to measure since AB·ATP·AA complexes are not stable because of phosphorylation of AA under these conditions. SPR measurements of the interaction of AB with the AA-S58A mutant of AA, which cannot be phosphorylated by AB, revealed a higher affinity in the presence of ATP than of ADP [5]. However,

the affinity of the AA-S58A mutant in the presence of ADP is lower than for the wildtype. We therefore could not directly use the values determined for complexes of AA-S58A with AB·ATP, and had to set the second off-rate to a lower, arbitrarily chosen value ($k_{off2} = 0.001 \text{ s}^{-1}$).

In the absence of nucleotides AA-AB binding is weak [19] and we used an off-rate that corresponds to a dissociation constant of 2.6 mM.

It was assumed that the presence of σ^F did not affect the AB·AA affinity [18].

σ^F -AB binding constants

The next group of constants for which SPR data have been published [5] are those that characterize the σ^F -AB interaction (59-93). While these could be used for the σ^F -AB·ATP interaction, fluorescence spectroscopy data suggest a lower σ^F ·AB·ADP affinity than that measured by SPR (Fig. 2A). Accordingly the σ^F ·AB·ADP off-rate was increased to 4 s^{-1} . To reproduce the kinetics of σ^F ·AB·ADP binding we have to assume that nucleotide-free AB can also interact weakly with σ^F ($k_{off} = 40 \text{ s}^{-1}$). The σ^F ·AB affinity in the presence of AA (77-93) was determined from fluorescence quenching data on AA-induced σ^F release. Fitting of the experimental data required the offrate with ATP present to be 100 times higher in the presence of AA than in its absence (a feature that had been noted previously [15]), and required an even higher off-rate in the presence of ADP. We set the off-rate in the presence of ADP to the value of the on-rate, thus assuming no binding, but smaller values for the off-rate would give similar simulation results.

Rates for AB conformational changes

The SPR experiments on AB-AA binding provide the only rates available for the interconversion between R and T-states, and we used the rate for the disfavoured direction (2 s^{-1}) throughout (116-137). In order to obtain allosteric behaviour, the favoured direction (94-115) when both monomers have symmetrical ligands must be attained faster than the rate estimated by SPR in the presence of ADP when only one monomer has bound AA (7.4 s^{-1}). We used $5 \times 10^3 \text{ s}^{-1}$. The exact value for this depends on the choice of the lid closure rate in the low affinity conformation (see below).

ADP-ATP exchange

The AB nucleotide binding pocket is partially covered by a flexible loop known as the “ATP-lid” [2]. ADP-ATP exchange (138-182) requires lid opening [18] and subsequent release of ADP and binding of ATP. The affinity of AB for ATP and ADP has been determined to be $K_D \sim 200 \mu\text{M}$ [20]. Fluorescence experiments suggest a slightly lower AB·ADP affinity [18]. Assuming that the on-rate for this interaction is in the range found for other associations between proteins and small ligands ($k_{on} \sim 10^7 \text{ M}^{-1}\text{s}^{-1}$ [17]) this gives $k_{off} \sim 2 \times 10^3 \text{ s}^{-1}$. ADP-ATP exchange has been found experimentally to proceed at a rate of about 1 s^{-1} . This is much slower than would be expected from the nucleotide on- and off-rates, and has been interpreted as the lid opening rate [18]. The nucleotide-bound monomer is predominantly in the low-affinity conformation, and lid opening in this conformation was therefore taken to proceed at 1 s^{-1} . Given the choice for the rate of the conformational change, the lid closure rate had to be set to $5 \times 10^5 \text{ s}^{-1}$ in order to reproduce the observed rebinding rate of σ^F ·AB complexes after the AA-induced σ^F release (Fig. 2B), in agreement with the intuitive consideration that

the lid should be predominately closed when nucleotides are bound. It should be noted that these several steps associated with ADP-ATP exchange were included in the model only when the level of detail of available experimental information required a similar level of detail in the model - otherwise only the rate-limiting steps were considered in order to reduce the complexity of the model.

AA phosphorylation and dephosphorylation rates

The phosphorylation of AA (183-192) exhibits a biphasic timecourse (Fig. 2 C) [21, 5]. The initial rate is equal to the AA phosphorylation rate, and the subsequent reduction in rate is due to the sequestering of AA and AB in AB·ADP·AA complexes. The phosphorylation rate of AA can thus be estimated from the initial slope of the biphasic phosphorylation reaction as 0.013 s^{-1} , a value that is close to previous estimates [22]. The rate of AA-P production when AB·ADP·AA complexes have already formed is much higher than the rate of dissociation of the AB·ADP·AA complex. ADP-ATP exchange must therefore be possible while AA is bound to AB·ADP (162-165) - though at a reduced rate. Modelling of the steady-state rate of phosphorylation requires a ADP-ATP exchange rate for AB·AA of $1.2 \times 10^{-3} \text{ s}^{-1}$ (Fig. 2C). ATP hydrolysis will be much slower than AA phosphorylation and was therefore ignored.

Interestingly, when AB is pre-incubated for 5 minutes with AA and $5\mu\text{M}$ ADP before addition of $100 \mu\text{M}$ ATP the biphasic phosphorylation timecourse can be directly transformed into a linear timecourse with the lower phosphorylation rate throughout (Fig. 2 C); by contrast, pre-incubation with $5\mu\text{M}$ ADP alone has only a minor effect (Fig. 2 C). From these results it can be concluded that ADP-AB binding is weak but can be facilitated by AA, which itself binds weakly to AB when no nucleotide is bound [19]. In order to obtain such weak AB-ADP binding (while retaining a high affinity once ADP is bound), the R state must be favoured when the lid is open; in this conformation AB must have a lower affinity for ADP ($k_{off} = 10^5 \text{ s}^{-1}$) and the lid must be less mobile, that is the lid opening and closure rates need to be of order 10^{-4} s^{-1} . The only exception to this is when σ^F is bound, when we have to assume a lid closure rate of 70 s^{-1} to reproduce $\sigma^F\text{-AB-ADP}$ binding (Fig. 2A). In order to limit the number of variables we ignored the (disfavoured) closed lid state of AB when no nucleotide is bound; instead we assumed that the R state was 50 times more abundant than we had assumed elsewhere in the model. This is important in order to reduce the fraction of AB in the open, nucleotide-free tense state, which has a higher affinity for ADP than the relaxed state. Note that these particular parameter choices are needed to reproduce the *in vitro* results shown in Figure 2 but have little or no impact on the other results shown.

Dephosphorylation of AA-P (193-195) *in vitro* with IIE domain III has been measured to proceed at 0.085 s^{-1} [23]. The on-rate for IIE·AA-P is unknown, as is the off-rate, and these were set to “standard” protein binding and unbinding rates, e.g. $10^6 \text{ M}^{-1}\text{s}^{-1}$ and 0.1 s^{-1} respectively.

Verification of the model by comparison to *in vitro* data

The model quantitatively reproduces experimental results of $\sigma^F\cdot AB$ sensitivity to variations in AA and IIE.

With all the kinetic parameters determined we first sought to reproduce recent biochemical *in vitro* results (shown as circles in Fig. 3 A) which revealed that $\sigma^F\cdot AB\cdot ATP$ complexes are highly sensitive to changes in IIE activity [9], thus lending support to the hypothesis that the septation-dependent increase in IIE activity may lead to σ^F release in the prespore [6]. Translation of the scheme into a set of coupled differential equations allowed us to reproduce quantitatively the high sensitivity of $\sigma^F\cdot AB\cdot ATP$ complexes to such changes in IIE activity, and also showed that the complexes are sensitive to changes in the AA concentration (compare 2.5 μM and 4 μM curves in Fig. 3 A). The model also captured the kinetics of $\sigma^F\cdot AB$ complex formation upon addition of ATP, the dissociation of the complex upon addition of AA and the effect of IIE on re-formation of the complex (Fig. 2C in the main paper). The considerable variation in the experimental timecourses (compare the three black curves for IIE=0 nM in Fig. 2C in the main paper) may be due to the high sensitivity of the kinetics to concentration. Comparison to the results in Fig. 2B suggests that the slower recovery rate found in the simulation is the more realistic one. The values for the steady-state dissociation of the complex are more robust, and the standard deviations between three independent experiments, as indicated by error bars in Figure 3A, are generally small. In both cases the modeling results are within the experimental range. The close fit of simulation and experiment, despite inherent experimental errors in the parameters including protein concentration, can be attributed to the robustness of the model (see below) and to the fact that the constants for the various on- and off-rates were all derived from similar experimental protocols.

The robustness of the mathematical model to variations in parameters.

The regulatory network can be regarded as robust if small changes in the parameter values lead to only small changes in the response. Given the availability of experimental data, the sensitivity of the model to variations in the kinetic parameters can be assessed by determining the deviation Δ_j of the simulation values s_i from the N experimental equilibrium results e_i (Fig. 3A) in response to a change in the kinetic parameter value k_j as

$$\Delta_j = \sqrt{\frac{1}{N} \sum_{i=1}^N \left(\frac{s_i - e_i}{e_i} \right)^2}. \quad (1)$$

Those reactions j , for which Δ_j did not increase by more than 1% when k_j was either set to zero or varied between 10^{-3} and 10^6 in multiples of 10 were considered insensitive. Those for which even a small (10-fold) change in the parameter led to an increase in Δ_j by more than 1% were considered sensitive. This analysis picks out nicely the key reaction pathways in the scheme and shows that relatively few reactions are sensitive to parameter variations. Sensitive reactions include the phosphorylation and dephosphorylation of AA, the binding of AA to $\sigma^F\cdot AB$ complexes and also those that lead to $AB\cdot ADP\cdot AA$ complex formation or ADP-ATP exchange.

Predictions of the effect of AB·ADP·AA complex formation.

AB·ADP·AA complex formation coincides with σ^F release from the σ^F ·AB·ATP complex (compare Fig. 3 A and B) and is important for the high sensitivity of σ^F release to changes in the AA concentration. The formation of AB·ADP·AA complexes also minimizes the need for cycling between AA and AA-P [5] and associated ATP consumption. Thus, the ATP consumption per minute per σ^F released does not increase monotonically with increasing IIE concentrations, but reaches a minimum (Fig. 3 B, dotted line) when sufficient unbound AA is available to sequester AB in AB·ADP·AA complexes (Fig. 3 B, solid line).

The AA-dependent trapping of AB·ADP in AB·ADP·AA complexes can be observed experimentally in the form of an increasing delay in σ^F ·AB complex re-formation when equimolar concentrations of AB and σ^F are mixed with increasing molar ratios of AA (Fig. 2D in the main paper). The non-linear increase in the delay times with increasing AA concentrations reflects the non-linear AA-dependence of AB·ADP·AA complex formation. It should be noted that the extent to which this delay increases with increasing AA concentration would be smaller if the AA-AB·ADP affinity were lower.

Application of the model to the sporulating cell *in vivo*

With a model that reproduces the *in vitro* data quantitatively we are now in a position to investigate the physiological situation. Relatively few alterations have to be made to the model to take account of the differences between the *in vitro* and *in vivo* conditions. The membrane location of IIE in the cell does not need to be considered explicitly in the model since, given the dimensions of the forespore, spatial concentration gradients on the timescale of the reactions would be expected to be negligible. A change has, however, to be made to the ATP and protein concentrations, which are higher *in vivo* at the time of septation than in the *in vitro* experiments. The ATP concentration was set to 1 mM because the lower end of the experimentally reported ATP concentration range (0.85 mM to 3 mM) for vegetative *B. subtilis* [24, 25, 26] is likely to apply to the starving sporulating condition. The ADP concentration was set to 100 μ M, which is a tenth of the ATP concentration. To simulate the experimentally observed time course of protein expression during sporulation [5, 27, 28] we started the sporulation reaction at time -120 minutes without protein and used an expression rate of 6×10^{-9} M s⁻¹ for AA and AB, whose translation has been suggested to be coupled [29], and 2×10^{-9} M s⁻¹ for σ^F and IIE (Fig. 4A). Septation (a 4-fold increase in IIE and associated AA-P) was introduced after 120 minutes [5, 27, 28] unless otherwise stated. The transient genetic imbalance, which arises upon septum formation and which results in the prespore lacking the *spoIIA* operon for 10-20 minutes after septation [7, 8], was modelled by prohibiting expression of AA, AB and σ^F for 15 minutes after septation. The emergence of unphosphorylated AA (Fig. 4B) further leads to repression of *spoIIE* and the *spoIIA* operon via inactivation of Spo0A [30]. Note that in agreement with experimental observations [31] almost half of all unbound AA (e.g. AA that is not bound to IIE) is unphosphorylated already before septation (Fig. 4B).

An amino-acid sequence in the extreme C-terminus of AB markedly increases the AB degradation rate *in vivo* [10]. In the simulations unbound AB was therefore associated with a degradation rate of 4.1×10^{-4} s⁻¹, which gives rise to the experimentally observed half-life of about 28 minutes [10].

The only rate constant that needs to be altered from the *in vitro* model is the IIE phosphatase rate, which experiments suggest is lower *in vivo* [32]. Modelling predicts that the reduction

needs to be by at least 10-fold to avoid septation-independent release of σ^F (Fig. 3A in the main paper); a 20-fold reduction is used in all simulation results presented here. This reduction can be partly accounted for by the different *in vivo* and *in vitro* concentrations of Mn^{2+} and Mg^{2+} . The phosphatase rate is substantially higher in the presence of Mn^{2+} [33]; but, given that the phosphatase rate has been determined in the presence of Mn^{2+} while Mg^{2+} predominates in the bacterial cell, the rate *in vivo* may be considerably smaller than the literature value. However, this is unlikely to account for a 10-fold (let alone a 20-fold) reduction, and it may be that further alterations must be made to the IIE environment or that an unknown IIE inhibitor exists [31, 32].

IIE accumulation on the septum, AB alloster and a short half-life enable compartment-specific gene transcription

While septal accumulation of IIE accumulation [6] and a short half-life of unbound AB [10] have been established experimentally as key components of the mechanism that enables prespore-specific σ^F release, it is unclear how they contribute and whether they are sufficient given that the IIE activity increase in the prespore is small and that the half-life of unbound AB strongly exceeds the time scale on which σ^F is activated. Moreover, it has so far been a paradox, how released σ^F can displace σ^A on the RNA polymerase despite the (unfavourable) competition of σ^F with the transcription factor σ^A [27].

We will show in the following that septal accumulation of IIE is sufficient because IIE accumulates on the septum together with its substrate AA-P; this increases the rate of AA formation by at least 2.5-fold. The here-described alloster of AB enables the high sensitivity to such small changes in AA production; degradation of unbound AB is important to tune the protein concentrations in a way that small changes can act as a trigger without rendering the regulatory network vulnerable to fluctuations in protein expression. The relative affinities of the RNA polymerase for σ^F and σ^A are shown to be optimized to allow for a coexistence of both holoenzymes. Other hypotheses such as the removal of a IIE inhibitor or effects of the transient genetic imbalance are shown to be irrelevant.

Accumulation of IIE (in association with its substrate AA-P) at the septum is sufficient to induce σ^F release in the prespore.

Contrary to previous suggestions, the model demonstrates that septal accumulation of IIE is sufficient to induce σ^F release in the prespore; it is not necessary to increase the IIE phosphatase rate in the prespore (for example by the removal of an inhibitor). As AA production is equal to the phosphatase rate times the concentration of IIE-AA-P complexes, it is sufficient to increase the substrate and enzyme concentrations by accumulation on the septum (Fig. 5A). Substrate and enzyme increase together when IIE accumulates on the septum because, owing to low phosphatase rate and the slightly higher total AA concentration relative to the IIE concentration in the cell, almost all IIE is associated with AA-P before septation (Fig. 3B in the main paper); enzyme and substrate would accumulate together on the septum even if the IIE-AA-P affinity were as low as micromolar.

An increase in either the IIE activity or AA-P concentration alone is far less efficient even if the phosphatase rate is set to the highest physiological possible value (Fig. 5 A). It is therefore

necessary for IIE to be present before septation, since that is the only way in which septal accumulation of IIE could also increase the AA concentration in the prespore. In fact asymmetric septation appears to require the presence of a significant IIE concentration [34, 35, 36, 37].

Formation of the σ^F -RNA polymerase holoenzyme

Prespore-specific σ^F release is only a first step to differential gene expression. In order to direct gene expression σ^F needs to bind to the RNA polymerase, from where it needs to displace σ^A . The mechanism of the latter has so far been unclear given the (unfavourable) competition of σ^F with σ^A (σ^A binds to the polymerase with a 25-fold higher affinity (560 nM and 22.5 nM for σ^F and σ^A respectively), but it is only slightly less abundant ($\sim 7.5\mu M$) than released σ^F [27]). As the core RNA polymerase concentration is comparatively high ($\sim 7.5\mu M$), the mathematical model predicts that micromolar concentrations of σ^F -RNAPol holoenzyme can form spontaneously in response to asymmetric septation (Fig. 3E in the main paper), and that these complexes co-exist with micromolar concentrations of σ^A -RNAPol holoenzyme (Fig. 3E in the main paper). The latter result is in agreement with the experimental observation that σ^A -RNAPol holoenzyme persists throughout the sporulation process [38].

Figure 3E in the main paper further shows that IIE (and AA-P bound to it) needs to increase by at least 2.5-fold in order to ensure the formation of micromolar σ^F -RNAPol concentrations. Given the difference in volume between the two compartments, accumulation of IIE on the septum will in fact lead to at least such an increase (see Supplementary Information). However, as discussed in the Supplementary Information, a 4-fold increase is a more realistic description of the sporulating cell and is therefore used in all the simulations presented here.

The role of the transient genetic imbalance

The view that σ^F release is driven by a change in IIE activity at the asymmetric septum has been challenged by the finding that σ^F was still released, albeit with a significant delay, in mutants where wild-type IIE was replaced by a soluble phosphatase domain (IIE Δ mem) [12]. The formation of σ^F -RNAPol in the IIE Δ mem mutant was subsequently shown to be enabled by the block in AB expression that follows septation due to a transient genetic imbalance [8].

The simulation correctly predicts the phenotype of mutants that lack the transient genetic imbalance and the impact of the IIE Δ mem on such background (Fig. 6A). Importantly however, the simulation also shows that a 10-20 minute block in AB expression (as may arise from the transient genetic imbalance - Fig. 6B) is insufficient to drive prespore specific σ^F release in IIE Δ mem mutants (Fig. 6C, compare solid and dotted lines). A continuous block in AB expression is necessary (Fig. 6C, solid line) and this cannot be achieved by Spo0A repression since, unlike wildtype, IIE Δ mem does not dephosphorylate sufficient AA upon septation (Fig. 6D).

We conclude that a genetic imbalance as short as 10-20 minutes cannot drive compartment specific gene expression. AB decay leads to σ^F release only after 30-40 minutes and therefore only enables significantly delayed σ^F release in IIE Δ mem mutants. Successful sporulation, however, requires that σ^F is released within 10 minutes after septation [1]. IIE accumulation on the septum is therefore necessary to enable rapid σ^F release. Additional mechanisms such as inhibitor removal [7] or a block in the release of dephosphorylated AA from IIE before septum formation [31] are not required.

The role of the short half-life for unbound AB

While results like those above question a role for a short half-life of unbound AB in rapid prespore-specific σ^F release, mutants with stable AB are sporulation deficient [10]. The simulation now reveals that the 28 minutes half-life of unbound AB is important to limit the AB concentration before septation (Fig. 3D in the main paper). The use of AB degradation rather than a lower expression rate is important to guarantee robustness to stochastic fluctuations in gene expression as is discussed below.

Allosteric behaviour of AB ensures both sensitivity and robustness

AB allostery is key to the high sensitivity to changes in the IIE·AA-P concentration and ensures that the system is robust to the initial parallel increases in the protein concentrations (Fig. 7A). Due to AB allostery σ^F ·AB complexes are stable at low AA concentration but become rapidly dissolved once the AA concentration reaches a critical threshold after septation. The premature formation of AB·AA complexes in the absence of allostery (Fig. 7B) would have two detrimental effects. First, sequestration of AB would free σ^F (Fig. 7A,B). Secondly, sequestration of AA would reduce the fraction of IIE that is bound by its substrate AA-P (Fig. 7C), thereby interfering with the simultaneous accumulation of IIE and AA-P when the septum forms, and thus limiting the formation of unphosphorylated AA in the prespore since - unlike in metabolic pathways - IIE's substrate (AA-P) is a protein and present at a low concentration in the cell.

We have investigated whether non-allosteric behaviour of AB could be compensated for by a stronger inhibition of IIE. However, the model shows that even a 1000-fold inhibition of IIE activity would be ineffective in preventing premature σ^F release (Fig 7, dashed lines) and would fail to provide for specific σ^F release in response to septation.

Economic efficiency through limiting ATP consumption

The avoidance of “ATP wastage” can be expected to become particularly important once nutrients are scarce as is the case at the onset of sporulation. The regulatory network that controls σ^F release is optimized to limit ATP wastage. Rapid formation of σ^F ·RNAPol holoenzyme (Fig. 8A) is accompanied by the accumulation of most of the AB in AB·ADP·AA complexes (Fig. 8B). If the simulation is altered so as to prohibit the formation of these complexes, AB accumulates instead in AB·ATP·AA complexes; but the consumption of ATP is then greatly increased (Fig. 4D in the main paper). We conclude that, for σ^F ·RNAPol holoenzyme to be formed and to persist without excessive waste of ATP, the formation of AB·ADP·AA complexes and the degradation of AB are both important. AB·ADP·AA complexes therefore play an important role in acting as a sink for AB after the increase in IIE (and associated AA-P) that occurs at asymmetric septation.

Robustness

Biological networks need to be organized in a way that they are sensitive to regulatory input but robust to the small variations that may arise from changes in environmental conditions or from stochastic fluctuations within the cell. The sporulation network meets both conditions to an

impressive degree. The protein concentrations are tuned to ensure a high sensitivity to changes in the IIE concentration while being robust to stochastic fluctuations in gene expression rates (Fig. 4A in the main paper). The additional robustness of the network to random changes in values in kinetic parameter and enzymatic rates (Fig. 9) justifies our approach of using the kinetic parameters that were determined from *in vitro* experiments. By means of control coefficients we determine the reactions that the regulatory network is most sensitive to as the phosphorylation and phosphatase steps.

Protein expression is tuned to ensure robustness

During the vegetative phase, the concentrations of σ^F , AA, AB, and IIE are too low to allow sufficient σ^F ·RNAPol formation to drive prespore development (Fig. 4A and Fig. 4B in the main paper). This efficiently protects the cell from premature σ^F activation. The triggering of differential gene expression requires the formation of IIE·AA-P complexes, and therefore the expression of AA and IIE, prior to septation (see above). In order to avoid premature σ^F activation all sporulation proteins (σ^F , AA, AB and IIE) need to be expressed in parallel prior to septation. Given the low numbers of proteins expressed, the process is inherently stochastic. The ratio between the proteins is essential to avoid spontaneous σ^F release, and translational coupling of all proteins is the best strategy to avoid failure (dashed line in Fig. 4A in the main paper). However, the downside of such coupling is that the ratios between proteins would then need to be established by degradation which is uneconomic. The simulation reveals that already the coupling of AA and AB translation strongly increases robustness as compared to a mechanism that does not involve coupling (compare dashed and dotted lines in Fig. 4A in the main paper).

The robustness will even be higher than suggested by Figure 4A in the main paper if the time point of septation depended on the protein (and in particular the IIE) concentration as may indeed apply to the cell [35, 37]. The impact of the timepoint on sporulation efficiency reflects the need to exceed a certain protein concentration before the septation-dependent increase in IIE·AA-P can trigger the formation of σ^F ·RNAPol at micromolar concentrations. The dotted line in Figure 4B in the main paper suggests this threshold to be 10 μ M for σ^F (and corresponding concentrations for the other proteins) at the timepoint of septation which is within the physiological concentration range for which σ^F ·RNAPol formation has been observed [5, 28]. We suggest that in order to avoid unproductive septation, the timing of septum formation must be linked to the overall concentration of the proteins relevant to sporulation; this may explain the large variance in the delay between the onset of sporulation and septation that is observed under different sporulation conditions. In the absence of a septation-dependent increase in the IIE·AA-P concentration the concentration of σ^F ·RNAPol remains too low to trigger downstream signaling (solid line in Fig. 4B in the main paper). This protects the mother cell, where the concentration of IIE·AA-P actually decreases slightly, from spontaneous σ^F release.

Critical parameters that determine the behaviour of the regulatory network

The impact of the individual kinetic parameters on the behaviour of the model can be assessed by means of control coefficients, as previously suggested for the analysis of signaling networks by Lee and co-workers [39]. Control coefficients can be used to quantify the relative change in

a model variable in response to (small) relative changes in a parameter value k_i . Here they were determined from

$$C_i^{RN\text{Apol}(\sigma^F)} = \frac{\delta RN\text{Apol}(\sigma^F)}{RN\text{Apol}(\sigma^F)} \frac{k_i}{\delta k_i}, \quad (2)$$

allowing the impact of parameter perturbations on the concentration of $\text{RN}\text{Apol}(\sigma^F)$ complexes to be ascertained. To understand the relative impact of the different interactions we studied the 30 independent rate constants listed in Tables 1&2. Control coefficients were determined in the equilibrium state before septation. We used $15 \mu\text{M } \sigma^F$, $30 \mu\text{M AA}$, $22.5 \mu\text{M AB}$, and $15 \mu\text{M IIE}$ for the concentrations of the sporulation proteins, which reflect the experimentally observed ratios between them and are within the experimental concentration range [5, 27, 28]. As required by the summation theorem for concentration control [40] they sum to zero. Several reactions exert strong control ($C_i^{RN\text{Apol}(\sigma^F)} \geq 1$), most notably AA phosphorylation and dephosphorylation, but the reactions responsible for ADP-ATP exchange and the binding of the transcription factors also have a strong effect (Tables 1&2).

Affinities of the transcription factor are particularly interesting since the relative affinities of σ^F and σ^A appeared counterintuitive when first determined [27]. The mathematical model now reveals that an equal, or higher, affinity of σ^F relative to σ^A for the RNA polymerase would result in a strong increase in $\text{RN}\text{Apol}(\sigma^F)$ complex formation even before septation, which could lead to premature activation (Fig. 3D in the main paper).

We conclude that several safeguards are employed to avoid premature activation of sporulation notwithstanding the high sensitivity of the regulatory system to small perturbations in protein concentration. These safeguards include a tight control of protein concentrations, an adjustment of the phosphatase rate, the different affinities of the RNA polymerase for the two transcription factors and the allosteric behaviour of AB.

Discussion

Complex biological networks are difficult to understand from verbal descriptions, and mathematical modelling is a promising tool to integrate the available information. However, realistic models cannot be built without quantitative experimental data. The system studied here offered several unusual advantages in that the entire regulatory network could be reconstituted *in vitro* and specific fluorescence probes were available to study all relevant interactions. This enabled realistic values for all kinetic parameters that affect the model to be estimated from experiments, and allowed the derivation of a very detailed model of the process that reproduced the experimental data quantitatively. In applying the model to the physiological situation the phosphatase rate of IIE, which exhibits a lower rate *in vivo* than *in vitro* [32], was the only parameter that had to be changed.

We began with a simple, basic circuit from published schemes but this rapidly grew into a large network after mathematical modeling predicted that AB is an allosteric protein. Here the combination of theory and experiment became particularly fruitful because theoretical predictions led to new experiments and analysis. Some rate constants, such as the phosphorylation rate and the $\sigma^F\text{-AB-ADP}$ binding rates, which had been estimated from previous experiments using simple models, also needed to be re-evaluated as the regulatory scheme became more complex. Once the rate and binding constants had been determined, the time-dependent variation in the system variables (e.g. concentrations of the pathway components and their complexes) could

be analysed by translating the interactions into a set of ordinary differential equations, which could be solved numerically. Comparison of the model predictions to data derived *in vitro* confirmed that the model was realistic and a perturbation study revealed that the model is robust to variations in the kinetic parameter values which justified a direct application of the model to the physiological situation.

Extrapolation of the model to the physiological situation enabled us to evaluate many effects that had been associated with the regulation of σ^F release in the prespore and to integrate them into a mechanistic picture of the regulatory process. We conclude from analysis of the model that IIE accumulation on the asymmetrically placed septum is sufficient to trigger prespore-specific σ^F release because IIE association with its substrate AA-P maximises AA production in the prespore while AB allostericity generates the required sensitivity. Thus, the volume difference between the two compartments (mother cell and prespore), AB allostericity together with the architecture of the regulatory network as well as the balanced concentrations of all sporulation proteins are the key factors that ensure compartmentalized gene expression during sporulation in *B. subtilis*. Alternative mechanisms such as a block in AB expression or the removal of an (elusive) IIE inhibitor, possibly through a transient genetic imbalance, are unlikely to be of major physiological relevance.

The regulatory system that leads to compartmentalized gene expression in *B. subtilis* is optimized in many ways. First of all the effect of the septation-induced difference in the ratio of surface area to volume is maximized between the two compartments by concentrating the phosphatase IIE on the asymmetric septum, that is on the common interface. Given the small size of the bacterium, a homogeneous distribution of IIE on the surfaces of both compartments would have led to only a small change in the relative phosphatase activities. Association of IIE and AA-P ensures a simultaneous increase in concentration of both enzyme and substrate in the prespore, which in turn ensures the strong increase in AA production that leads to σ^F release. Secondly, the protein concentrations are tuned such that minute changes in IIE and AA can tip the balance while robustness to fluctuations in gene expression is ensured by coupled expression combined with protein degradation. Thirdly, the previously unnoticed allosteric behaviour of the AB dimer enables the high sensitivity to changes in IIE and AA and at the same time prevents premature AB·ADP·AA complex formation, which would lead to σ^F release. Finally, the formation of AB·ADP·AA complexes after septation serves as sophisticated mechanism for preventing σ^F from rebinding to the released AB, thus providing rapid and prolonged σ^F release while minimizing cycling and associated wastage of ATP. AB·ADP·AA complexes thus serve to remove AB (AB sink [41, 42]) rather than AA (AA sink [43]).

The model's prediction that pre-septational AB·AA complex formation is detrimental and that AB·ADP·AA complexe serve as AA sink stands in direct opposition to the suggestion that AB·ADP·AA complexes may act as an AA sink to prevent premature σ^F release [43]. This suggestion had been proposed to explain the counterintuitive experimental observation that unphosphorylated AA can be observed long before septation but without inducing σ^F -dependent gene transcription [31]. Our model explains the pre-septational accumulation of (inactive) AA without invoking AB·ADP·AA complex formation (Fig. 4B, 7B). The large fraction of AA that is unphosphorylated at the very onset of sporulation (Fig. 4B) is the consequence of the low protein concentrations which prevent the formation of protein complexes; lack of AB·ATP·AA complex prevents AA phosphorylation. Similarly, most of the σ^F is free at that time, but its concentration is too low to allow the formation of sufficient σ^F ·RNA polymerase holoenzyme to effect gene transcription. Once protein concentrations increase, the model predicts that much AA will be bound in complexes with AB·ATP. Experiments find that half of AA is unphosphorylated already before septation, and the simulations predict that this applies indeed to the

soluble AA pool (not IIE bound).

The critical importance of the simultaneous accumulation of IIE and its substrate AA-P as well as the need to render septation dependent on the protein (and in particular IIE) concentration would probably have remained unnoticed without mathematical modeling. Much the contrary it had already been reasoned that the release of the product AA from IIE was inhibited before septation [31].

The mathematical model also resolves the paradox of why degradation of unbound AB is necessary for sporulation while the half-life (~ 28 minutes) strongly exceeds the time scale on which σ^F needs to be released (~ 10 minutes) [10, 1]. The model reveals that the observed half-life reduces the AB concentration, whose expression is presumably coupled with AA [29], to a level that small changes in the AA concentration can trigger σ^F release. Coupled expression and degradation of unbound AB (rather than all AB) confer robustness to fluctuations in gene expression. AB allostery ensures robustness to parallel changes in protein concentration (without this feature the initial increase in protein concentration might cause σ^F release in the entire sporangium). A IIE dependency of septation is likely to ensure that sufficient protein has been expressed such that septation can trigger the formation of micromolar σ^F ·RNAPol holoenzyme concentrations. The relative affinities of the transcription factors σ^F and σ^A for the core RNA polymerase are tuned to prevent premature activation whilst enabling the system to be triggered by small perturbations. Moreover RNAPol(σ^A) holoenzyme remains present when RNAPol(σ^F) emerges, in such a way that general transcription programs can still be carried out. The robustness of the regulatory circuit to alterations in concentration and values of kinetic parameters is such that the process can be deregulated only by mutation.

We conclude that the regulatory circuit described here appears to be optimized to the needs of the organism. It is tuned to ensure both high sensitivity to stimuli and robustness to random fluctuations. We show that the dimeric, allosteric kinase SpoIIAB plays a crucial role by enabling sensitivity, robustness, and minimal ATP consumption. The high sensitivity to changes in the IIE·AA-P concentration enables the two different developmental programs to be triggered by small concentration changes (such as can be induced by asymmetric septation) and with minimal ATP consumption.

While asymmetric cell division, and the resulting difference between the two compartments, is an elegant mechanism for achieving compartmentalized gene expression, other symmetry-breaking mechanisms must exist to induce compartmentalized gene expression in those sporulating bacteria, such as *Sporosarcina ureae*, that divide symmetrically during sporulation [44]. A deeper insight into such alternative mechanisms will be of great interest.

Appendix: Comments on how to estimate of septation-dependent IIE activity change

Given that IIE accumulates on the septum (together with any AA-P that is bound to it) the number of IIE·AA-P complexes acting per unit volume increases in the prespore and decreases in the mother cell. A lower limit for the septation-dependent increase in IIE activity in the prespore can be determined by assuming a) that all the IIE locates, together with its substrate, on to the septum in such a way that its activity is displayed equally on both faces and b) that the cell is cuboid.. Insertion of a septum at an x th of the length of the cuboid will give rise to two compartments, with the smaller having an x th of the total volume. If half of all IIE·AA-P is present in the smaller volume then there is an effective $\frac{x}{2}$ -fold increase in IIE·AA-P per unit volume of the smaller compartment. Septa form at one-fifth or less of the length of the cell [45] and the minimal increase in IIE activity is therefore 2.5.

In fact, each of the assumptions mentioned above underestimates the probable increase in IIE activity: the total quantity of IIE is slightly greater on the prespore face than on the mother-cell face of the septum [46, 31]; and the prespore is not a cuboid but has rounded ends [47]. Thus, although a 2.5-fold increase in IIE activity is sufficient to ensure the formation of enough σ^F ·RNAPol to permit transcription in the prespore (Fig. 5C), the 4-fold increase that we have assumed throughout this paper is a more realistic representation of the physiological situation.

References

- [1] Hilbert, D. W & Piggot, P. J. (2004) Compartmentalization of gene expression during *Bacillus subtilis* spore formation *Microbiol Mol Biol Rev* 68:234–262.
- [2] Campbell, E. A, Masuda, S, Sun, J. L, Muzzin, O, Olson, C. A, Wang, S, & Darst, S. A. (2002) Crystal structure of the *Bacillus stearothermophilus* anti-sigma factor SpoIIAB with the sporulation sigma factor σ^F *Cell* 108:795–807.
- [3] Ho, M, Carniol, K, & Losick, R. (2003) Evidence in support of a docking model for the release of the transcription factor σ^F from the antisigma factor SpoIIAB in *Bacillus subtilis*. *J Biol Chem* 278:20898–20905.
- [4] Masuda, S, Murakami, K. S, Wang, S, Anders Olson, C, Donigian, J, Leon, F, Darst, S. A, & Campbell, E. A. (2004) Crystal structures of the ADP and ATP bound forms of the *Bacillus* anti-sigma factor SpoIIAB in complex with the anti-anti-sigma SpoIIAA *J Mol Biol* 340:941–956.
- [5] Magnin, T, Lord, M, & Yudkin, M. (1997) Contribution of partner switching and SpoIIAA cycling to regulation of σ^F activity in sporulating *Bacillus subtilis*. *J Bacteriol* 179:3922–3927.
- [6] Duncan, L, Alper, S, Arigoni, F, Losick, R, & Stragier, P. (1995) Activation of cell-specific transcription by a serine phosphatase at the site of asymmetric division. *Science* 270:641–644.
- [7] Frandsen, N, Barák, I, Karmazyn-Campelli, C, & Stragier, P. (1999) Transient gene asymmetry during sporulation and establishment of cell specificity in *Bacillus subtilis*. *Genes Dev* 13:394–399.
- [8] Dworkin, J & Losick, R. (2001) Differential gene expression governed by chromosomal spatial asymmetry. *Cell* 107:339–346.
- [9] Clarkson, J, Campbell, I. D, & Yudkin, M. D. (2004) Efficient regulation of σ^F , the first sporulation-specific sigma factor in *B. subtilis*. *J Mol Biol* 342:1187–1195.
- [10] Pan, Q, Garsin, D, & Losick, R. (2001) Self-reinforcing activation of a cell-specific transcription factor by proteolysis of an anti-sigma factor in *B. subtilis*. *Mol Cell* 8:873–883.
- [11] Wu, Y, Nadler, M, Brennan, L, Gish, G, Timms, J, Fusaki, N, Jongstra-Bilen, J, Tada, N, Pawson, T, Wither, J, Neel, B, & Hozumi, N. (1998) The B-cell transmembrane protein CD72 binds to and is an in vivo substrate of the protein tyrosine phosphatase SHP-1. *Curr Biol* 8:1009–1017.
- [12] Arigoni, F, Guérout-Fleury, A, Barák, I, & Stragier, P. (1999) The SpoIIIE phosphatase, the sporulation septum and the establishment of forespore-specific transcription in *Bacillus subtilis*: a reassessment. *Mol Microbiol* 31:1407–1415.
- [13] Duncan, L & Losick, R. (1993) SpoIIAB is an anti-sigma factor that binds to and inhibits transcription by regulatory protein σ^F from *Bacillus subtilis* *Proc Natl Acad Sci U S A* 90:2325–2329.

- [14] Min, K. T, Hilditch, C. M, Diederich, B, Errington, J, & Yudkin, M. D. (1993) σ^F , the first compartment-specific transcription factor of *B. subtilis*, is regulated by an anti-sigma factor that is also a protein kinase *Cell* 74:735–742.
- [15] Clarkson, J, Campbell, I. D, & Yudkin, M. D. (2004) Physical evidence for the induced release of the *Bacillus subtilis* transcription factor, σ^F , from its inhibitory complex *J Mol Biol* 340:203–209.
- [16] Arigoni, F, Duncan, L, Alper, S, Losick, R, & Stragier, P. (1996) SpoIIIE governs the phosphorylation state of a protein regulating transcription factor σ^F during sporulation in *Bacillus subtilis*. *Proc Natl Acad Sci U S A* 93:3238–3242.
- [17] Fersht, A. (1998) *Structure and Mechanism in Protein Science*. (W.H. Freeman and Company).
- [18] Clarkson, J, Shu, J.-C, Harris, D. A, Campbell, I. D, & Yudkin, M. D. (2004) Fluorescence and kinetic analysis of the SpoIIAB phosphorylation reaction, a key regulator of sporulation in *Bacillus subtilis* *Biochemistry* 43:3120–3128.
- [19] Clarkson, J, Campbell, I. D, & Yudkin, M. D. (2001) NMR studies of the interactions of SpoIIAA with its partner proteins that regulate sporulation in *Bacillus subtilis* *J Mol Biol* 314:359–364.
- [20] Lord, M, Magnin, T, & Yudkin, M. D. (1996) Protein conformational change and nucleotide binding involved in regulation of σ^F in *Bacillus subtilis*. *J Bacteriol*. 178:6730–6735.
- [21] Najafi, S. M, Harris, D. A, & Yudkin, M. D. (1997) Properties of the phosphorylation reaction catalyzed by SpoIIAB that help to regulate sporulation of *Bacillus subtilis* *J Bacteriol* 179:5628–5631.
- [22] Shu, Clarkson, J, & Yudkin, M. D. (2004) Studies of SpoIIAB mutant proteins elucidate the mechanisms that regulate the developmental transcription factor σ^F in *Bacillus subtilis*. *Biochem J*. 384:169–178.
- [23] Lucet, I, Feucht, A, Yudkin, M, & Errington, J. (2000) Direct interaction between the cell division protein FtsZ and the cell differentiation protein SpoIIIE. *EMBO J* 19:1467–1475.
- [24] Jolliffe, L. K, Doyle, R. J, & Streips, U. N. (1981) The energized membrane and cellular autolysis in *Bacillus subtilis* *Cell* 25:753–763.
- [25] Guffanti, A. A, Clejan, S, Falk, L. H, Hicks, D. B, & Krulwich, T. A. (1987) Isolation and characterization of uncoupler-resistant mutants of *Bacillus subtilis* *J Bacteriol* 169:4469–4478.
- [26] Hecker, M, Heim, C, Volker, U, & Wolfel, L. (1988) Induction of stress proteins by sodium chloride treatment in *Bacillus subtilis* *Arch Microbiol* 150:564–566.
- [27] Lord, M, Barillà, D, & Yudkin, M. (1999) Replacement of vegetative σ^A by sporulation-specific σ^F as a component of the RNA polymerase holoenzyme in sporulating *Bacillus subtilis*. *J Bacteriol* 181:2346–2350.

[28] Lucet, I, Borriss, R, & Yudkin, M. (1999) Purification, kinetic properties, and intracellular concentration of SpoIIE, an integral membrane protein that regulates sporulation in *Bacillus subtilis*. *J Bacteriol* 181:3242–3245.

[29] Fort, P & Piggot, P. J. (1984) Nucleotide sequence of sporulation locus spoIIA in *Bacillus subtilis* *J Gen Microbiol* 130 (Pt 8):2147–2153.

[30] Arabolaza, A, Nakamura, A, Pedrido, M, Martelotto, L, Orsaria, L, & Grau, R. (2003) Characterization of a novel inhibitory feedback of the anti-anti-sigma SpoIIAA on Spo0A activation during development in *Bacillus subtilis*. *Mol Microbiol* 47:1251–1263.

[31] King, N, Dreesen, O, Stragier, P, Pogliano, K, & Losick, R. (1999) Septation, dephosphorylation, and the activation of σ^F during sporulation in *Bacillus subtilis*. *Genes Dev* 13:1156–1167.

[32] Feucht, A, Abbotts, L, & Errington, J. (2002) The cell differentiation protein SpoIIE contains a regulatory site that controls its phosphatase activity in response to asymmetric septation. *Mol Microbiol* 45:1119–1130.

[33] Schroeter, R, Schlisio, S, Lucet, I, Yudkin, M, & Borriss, R. (1999) The *Bacillus subtilis* regulator protein SpoIIE shares functional and structural similarities with eukaryotic protein phosphatases 2C *FEMS Microbiol Lett* 174:117–123.

[34] Barák, I & Youngman, P. (1996) SpoIIE mutants of *Bacillus subtilis* comprise two distinct phenotypic classes consistent with a dual functional role for the SpoIIE protein *J Bacteriol* 178:4984–4989.

[35] Khvorova, A, Zhang, L, Higgins, M. L, & Piggot, P. J. (1998) The spoIIE locus is involved in the Spo0A-dependent switch in the location of FtsZ rings in *Bacillus subtilis* *J Bacteriol* 180:1256–1260.

[36] Feucht, A, Daniel, R. A, & Errington, J. (1999) Characterization of a morphological checkpoint coupling cell-specific transcription to septation in *Bacillus subtilis* *Mol Microbiol* 33:1015–1026.

[37] Ben-Yehuda, S & Losick, R. (2002) Asymmetric cell division in *B. subtilis* involves a spiral-like intermediate of the cytokinetic protein FtsZ *Cell* 109:257–266.

[38] Fujita, M & Sadaie, Y. (1998) Rapid isolation of RNA polymerase from sporulating cells of *Bacillus subtilis* *Gene* 221:185–190.

[39] Lee, E, Salic, A, Kruger, R, Heinrich, R, & Kirschner, M. W. (2003) The roles of APC and axin derived from experimental and theoretical analysis of the Wnt pathway *PLoS Biol* 1:E10.

[40] Heinrich, R & Rapoport, T. A. (1974) A linear steady-state treatment of enzymatic chains. General properties, control and effector strength *Eur J Biochem* 42:89–95.

[41] Lee, C. S, Lucet, I, & Yudkin, M. D. (2000) Fate of the SpoIIAB*-ADP liberated after SpoIIAB phosphorylates SpoIIAA of *Bacillus subtilis* *J Bacteriol* 182:6250–6253.

- [42] Lee, C. S, Clarkson, J, Shu, J. C, Campbell, I. D, & Yudkin, M. D. (2001) *Bacillus subtilis* mutations that alter the pathway of phosphorylation of the anti-anti- σ^F factor SpoIIAA lead to a Spo- phenotype Mol Microbiol 40:9–19.
- [43] Carniol, K, Eichenberger, P, & Losick, R. (2004) A threshold mechanism governing activation of the developmental regulatory protein σ^F in *Bacillus subtilis* J Biol Chem 279:14860–14870.
- [44] Zhang, L, Higgins, M. L, & Piggot, P. J. (1997) The division during bacterial sporulation is symmetrically located in Sporosarcina ureae Mol Microbiol 25:1091–1098.
- [45] Illing, N & Errington, J. (1991) Genetic regulation of morphogenesis in *Bacillus subtilis*: roles of σ^E and σ^F in prespore engulfment J Bacteriol 173:3159–3169.
- [46] Wu, L. J, Feucht, A, & Errington, J. (1998) Prespore-specific gene expression in *Bacillus subtilis* is driven by sequestration of SpoIIE phosphatase to the prespore side of the asymmetric septum Genes Dev 12:1371–1380.
- [47] Ryter, A. (1965) Étude morphologique de la sporulation de *Bacillus subtilis*. Ann Inst Pasteur (Paris) 108:40–60.

Acknowledgements We thank J-C Shu for providing unpublished SPR data. This work was supported by the BBSRC UK. D.I. is a Junior Research Fellow at St John's College, University of Oxford and is supported by an EPSRC scholarship. I.D.C. acknowledges financial support from the Wellcome Trust and the NIH funded Cell Migration Consortium.

Figures

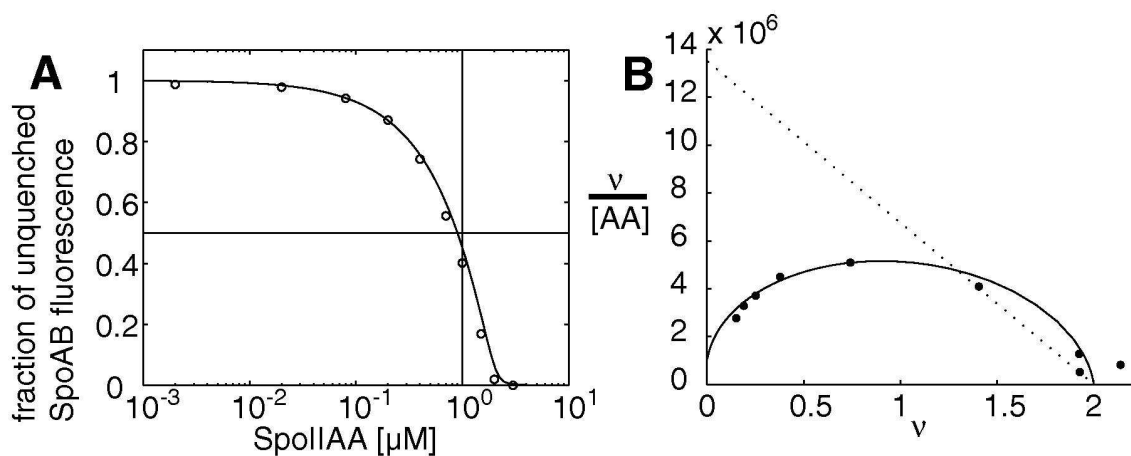


Figure 1: **SpoIAB is an allosteric protein.** (A) Fraction of AB (1 μM total) unbound as a function of the concentration of AA in the presence of 100 μM ADP, as determined by fluorescence quenching experiments with fluorescent mutant AB-F97W [18]. The points show previously unpublished experimental results; the line represents the binding curve expected from the kinetic constants employed in the mathematical model (which includes allostery of AB). (B) Scatchard plot obtained by determining the fraction of bound AB (ν) when 4 μM AA-S58A is mixed with different concentrations of AB. The points show previously unpublished experimental results; the lines represent the predicted Scatchard plot based on the assumption that AB is an allosteric protein (continuous line) or non-allosteric (dotted) with an affinity for AA-S58A·AB 3.7 times less than for AB·AA (Table 1). Note that a 1.3-fold higher AB concentration than measured had to be used to keep $\nu \leq 2$.

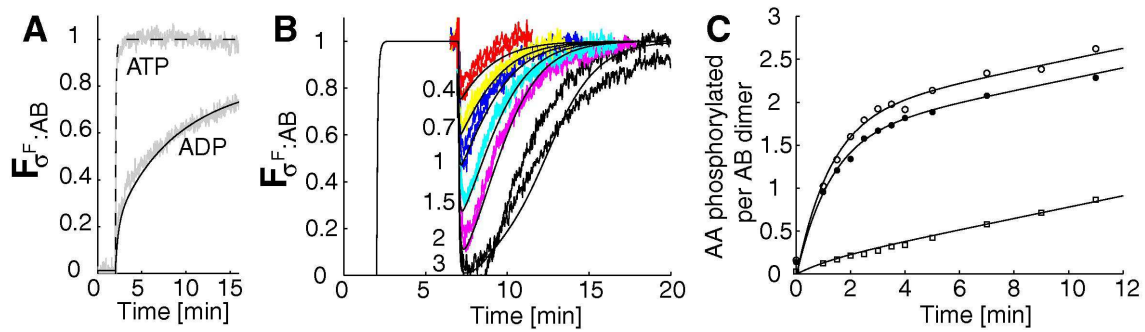


Figure 2: Estimate of parameter values. (A) Interactions between $1.3 \mu\text{M} \sigma^F$ and $1 \mu\text{M} \text{AB}$. The results of fluorescence quenching experiments [9] are shown as output from a recorder, and simulations are shown as smooth lines, either dashed (for ATP-dependent interactions) or continuous (for ADP-dependent interactions). (B) σ^F release from $\text{AB}\cdot\text{ATP}$ upon addition of AA. The results from two experiments are shown for the disruption of $\sigma^F\cdot\text{AB}$ complexes by 0.4 (red); 0.7 (yellow); 1 (blue); 1.5 (cyan); 2 (magenta); 3 (black) μM AA. The corresponding simulations are shown in smooth black lines, which are labeled with the relevant concentrations of AA. Experiments were carried out as described in [9] with the fluorescent mutant $\sigma^F\text{-W46L}$. (C) Phosphorylation of AA by AB when AB is directly incubated with $40 \mu\text{M}$ AA and $100 \mu\text{M}$ ATP (\circ) or pre-incubated for 5 minutes with either $5 \mu\text{M}$ ADP (\bullet) or $5 \mu\text{M}$ ADP and $40 \mu\text{M}$ AA (\square). The symbols show the experimental results [18], normalised by the factor 1.3 to take account of inaccuracies in the protein determination (see main text). The lines show the predictions of the mathematical model.

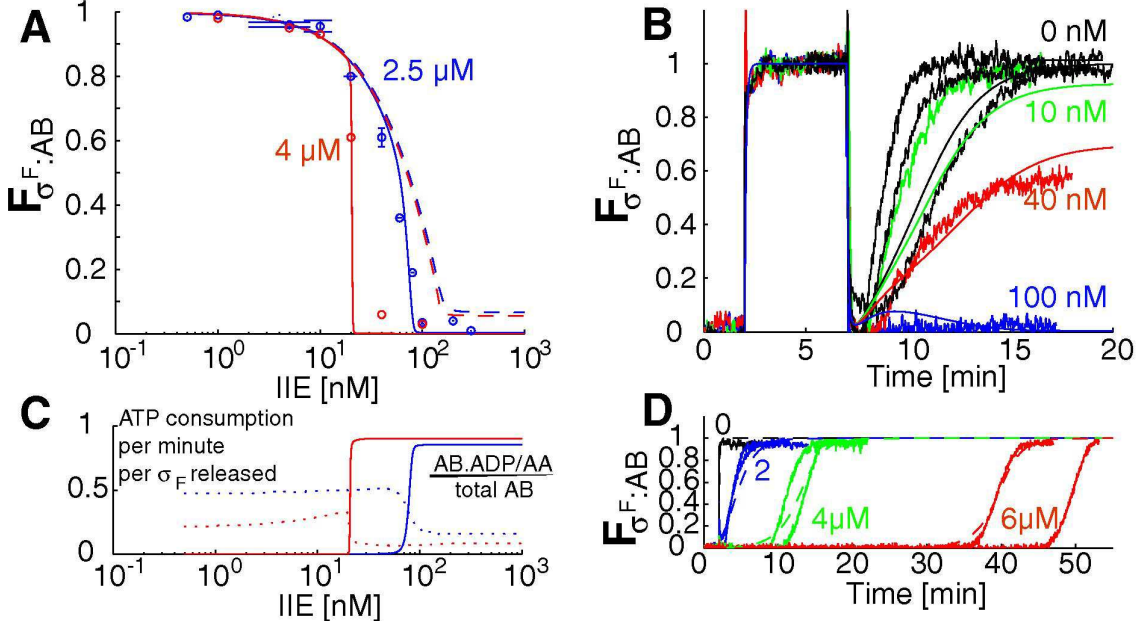


Figure 3: The dissociation of $\sigma^F\text{-AB}$ complexes is sensitive to changes in the concentration of IIE and AA. (A) Steady state after IIE-dependent dissociation of $\sigma^F\text{-AB-ATP}$ (1.3 μM σ^F , 1 μM AB dimer) in the presence of 2.5 μM (blue) or 4 μM (red) AA. Circles represent experimental results [9]. Continuous lines show the predictions of the mathematical model, which includes the formation of the AB·ADP·AA complex. Dashed lines show simulations based on the assumption that the formation of such a complex is impossible. (B) Kinetics of IIE-dependent dissociation of $\sigma^F\text{-AB-ATP}$ (1.3 μM σ^F , 1 μM AB dimer) in the presence of 2.5 μM AA, in the absence of IIE (black lines) or with 10 (green), 40 (red) or 100 (blue) nM IIE. Experimental results are taken from [9], and are shown as output from a recorder. Note that three experiments were run in the absence of IIE. The smooth continuous lines show simulations from the mathematical model. (C) Simulations of the proportion of AB sequestered into AB·ADP·AA complexes (continuous line) and ATP consumption per minute per σ^F released (dotted line) in the presence of 2.5 μM (blue) or 4 μM (red) AA. (D) $\sigma^F\text{-AB}$ complex formation on mixing of 1 μM AB and 1.3 μM σ^F with no (black), 2 μM (blue), 4 μM (green), or 6 μM (red) AA. Experimental results (two for each concentration of AA) are taken from [9] and are shown as output from a recorder; the dashed lines show simulations from the mathematical model at the same concentrations of AA.

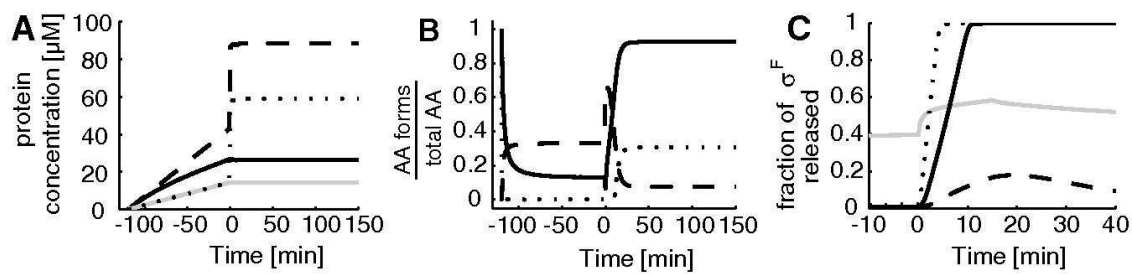


Figure 4: The simulation reproduces the experimentally observed concentrations of sporulation proteins. (A) Increase in the concentration of sporulation proteins during sporulation (AA- dashed; AB - continuous black; IIE - dotted; σ^F - grey). **(B)** Time-dependent fraction of AA that is unphosphorylated (solid line), unbound and unphosphorylated (dotted line) or bound in IIE·AA-P complexes (dashed line). In both panels, sporulation-dependent protein expression is started at -120 minutes; a four-fold increase in IIE and associated AA-P (to simulate the effect of asymmetric septation) is introduced at t=0. **(C)** Fraction of σ^F released in simulations based on the assumption that the IIE activity *in vivo* was not inhibited (continuous grey line), or inhibited by 10 (dotted), 20 (continuous black) or 40 times (dashes) compared with the maximum IIE activity measured *in vitro*. A four-fold increase in IIE and associated AA-P (to simulate the effect of asymmetric septation) is introduced at t=0.

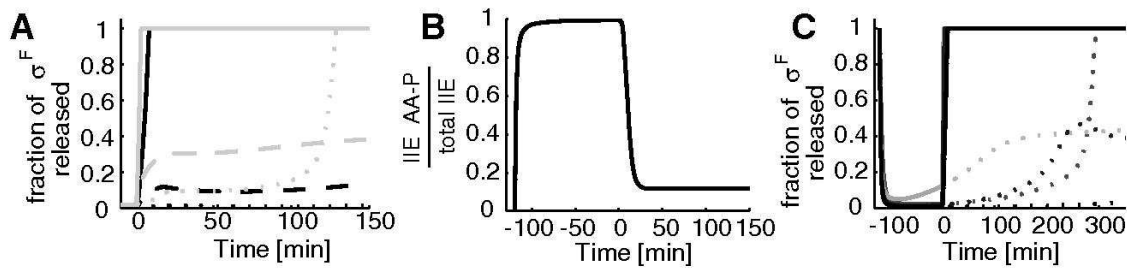


Figure 5: Simulations showing that a septation-dependent increase in IIE-AA-P is sufficient for σ^F release. (A) σ^F release in response to a 4-fold increase in IIE alone (dashes) in AA-P alone (dotted), or in IIE and AA-P (continuous line) imposed at $t=0$. The IIE phosphatase rate was either 10-times (grey) or 20-times (black) smaller than *in vitro*. **(B)** Time-dependent fraction of IIE in IIE-AA-P complexes. **(C)** Time-dependent σ^F release in wildtype (black), when AB expression is reduced by 30% (red line), if IIE expression is increased by two-fold (green and blue lines) and if IIE activity is increased by two-fold (green line). In all panels, the septum was assumed to form at $t=0$ (see main text).

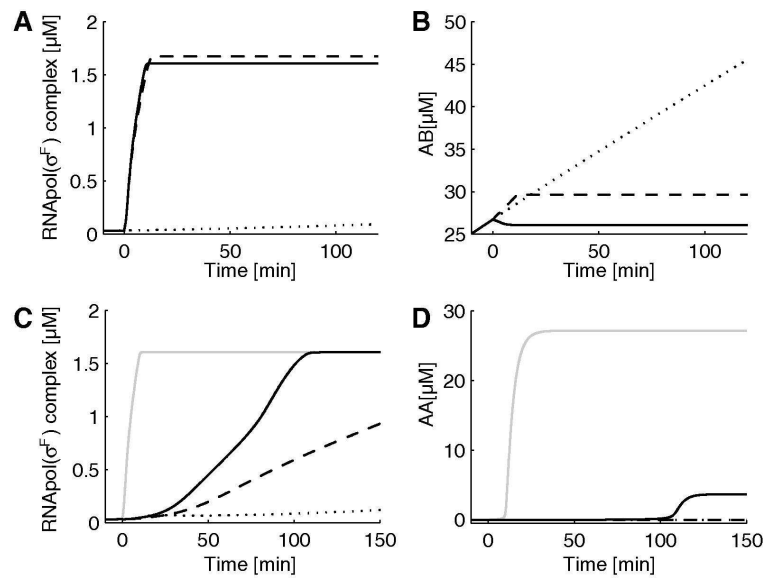


Figure 6: The effect of a transient genetic imbalance on σ^F release. (A) Formation of RNApol(σ^F) complexes, (B) total AB concentration for wt (continuous line) *spoIIAB*(ori) (dashes) *IIEΔmem* & *spoIIAB*(ori) (dotted). (C) Formation of RNApol(σ^F) complexes, (D) total AA concentration for wt (continuous grey line), for *IIEΔmem* if chromomosome translocation is blocked (solid line) if *Spo0A* is constitutively repressed (dashed line) or if *IIEΔmem* & *spoIIAB*(ori) (dotted). In all panels, the septum was assumed to form at t=0 (see main text).

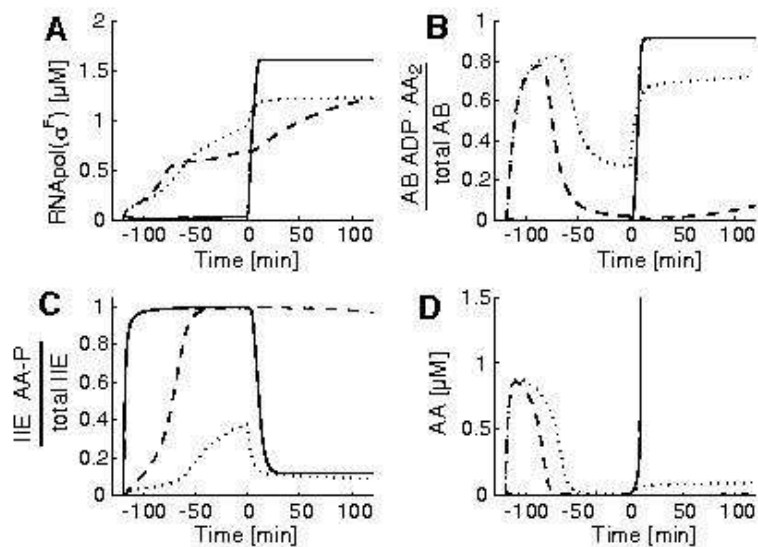


Figure 7: The allosteric behaviour of AB is necessary for successful sporulation. (A) The formation of RNApol(σ^F) holoenzyme, (B) the fraction of AB in AB·ADP·AA complexes, (C) the fraction of IIE in IIE·AA-P complexes, and (D) the fraction of unphosphorylated AA if AB is allosteric (continuous line) or not allosteric and the activity of IIE is inhibited 20-fold (dotted) or 1000-fold (dashes) compared with the maximum activity measured *in vitro*. A four-fold increase in IIE, together with its associated AA-P, is imposed at t= 0.

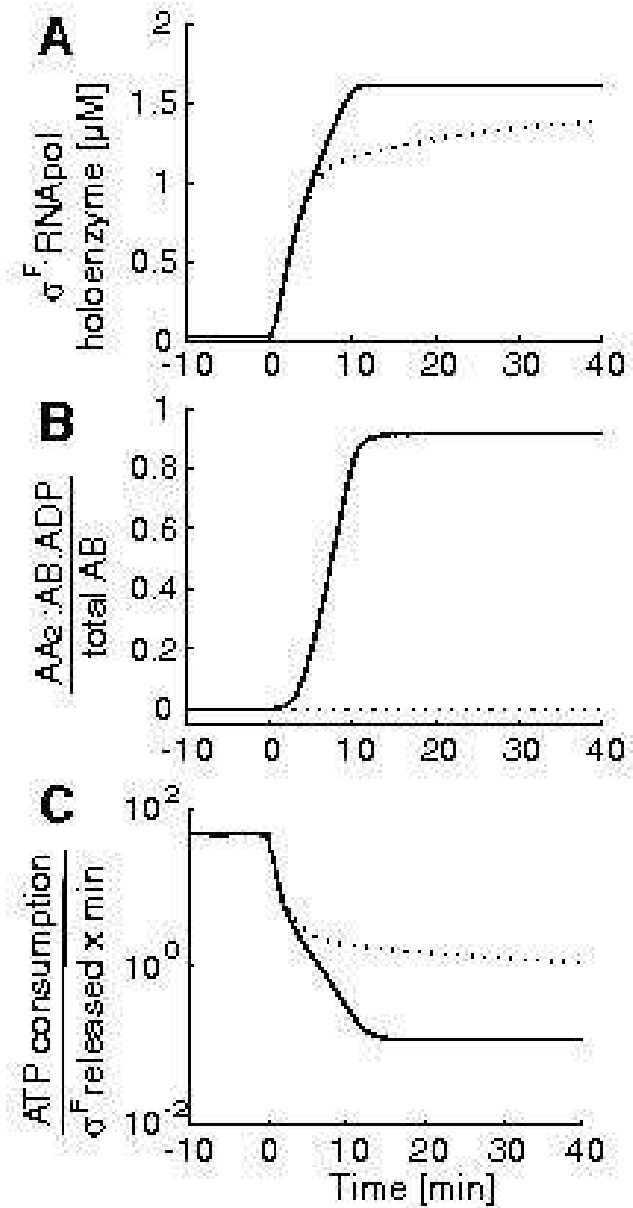


Figure 8: AB-ADP-AA complexes form upon asymmetric septation. The simulations show the effect of a four-fold increase at $t=0$ min of IIE, together with its associated AA-P, on (A) formation of σ^F -holoenzyme, (B) fraction of AB in $\text{AA}_2\text{-AB-ADP}$ complexes. (C) ATP consumption per minute per σ^F released for wildtype (continuous line) or for a variant in which AB-ADP-AA cannot be formed (dotted).

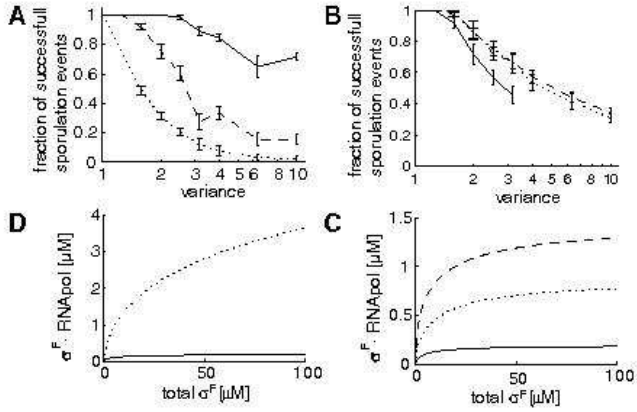


Figure 9: The robustness of the regulatory network. **(A)** The fraction of successful sporulation events if the rates of protein expression are varied randomly by the factor given on the x-axis and all expression rates are coupled (-), AA and AB expression is coupled (· · ·), all expression rates are varied randomly, the AB expression rate is $4 \times 10^{-9} \text{ M s}^{-1}$ and there is no AB degradation (---). A successful sporulation event was defined as one for which the concentration of RNA polymerase bound to F is lower than $0.4 \mu\text{M}$ before, and higher than $1 \mu\text{M}$ after, septation. Standard deviations are based on 10 sets of 100 runs each. **(B)** Fraction of successful sporulation events if either all binding rates (dashed), all enzymatic rates (dotted), all binding and enzymatic rates (solid) are varied randomly by the factor given on the x-axis. Standard deviations are based on 10 sets of 100 runs each; successful sporulation events are defined as those with a concentration of RNA polymerase(σ^F) holoenzyme less than $0.4 \mu\text{M}$ without, and greater than $1 \mu\text{M}$ with, a 4-fold increase in IIE (and associated AA-P). **(C)** Concentration of RNA polymerase(σ^F) holoenzyme as a function of the reference protein concentrations (as exemplified by the σ^F concentration). The relative concentration of IIE (and the associated AA-P) was either increased by four-fold (continuous line) or left unchanged (dotted). **(D)** Concentration of RNA polymerase σ^F holoenzyme if the affinities of the core RNA polymerase for σ^F and σ^A were as in the wild type (continuous line) or made equal by varying the rate of dissociation of either the σ^F holoenzyme ($k_{off}(\sigma^F) = 0.02 \text{ s}^{-1}$ - dashes) or the σ^A holoenzyme ($k_{off}(\sigma^A) = 0.55 \text{ s}^{-1}$ - dotted).

Tables

Table 1: **Control coefficients for the kinetic rate constants employed in the *in vitro* and *in vivo* simulations.** The determination of control coefficients $C_j^{RN\text{Apol}(\sigma^F)}$ is described in the main text. References to a particular figure show that a parameter value was derived from results presented in that figure rather than from previously published results.

rates	$C_j^{RN\text{Apol}(\sigma^F)}$
AA-AB on-rate	2×10^{-5}
AA-AB off-rate	-0.07
AA- $\hat{A}B$.ATP off-rate	0.03
AA- $\hat{A}B$.ADP off-rate	-0.02
AA- $\hat{A}B$ off-rate	5×10^{-7}
σ^F -AB on-rate	-0.66
σ^F -AB·ATP off-rate	0.29
σ^F -AB·ADP off-rate	10^{-3}
σ^F -AB· off-rate	-3×10^{-4}
σ^F -AB·ATP·AA off-rate	0.15
σ^F -AB·ADP·AA off-rate	10^{-6}
AB conformational change	-0.84
AB conformational change	0.08
AB conformational change	-0.08
lid opening T state	-1.16
lid opening R state	-9×10^{-6}
lid closure T state	1.14
lid closure R state	4×10^{-7}
lid closure R state (σ^F bound)	3×10^{-4}
nucleotide-AB on-rate	-5×10^{-4}
nucleotide-AB off-rate	-0.32
ADP-AB off-rate (T state)	-3×10^{-3}
ATP-ADP exchange for AB·AA	-6×10^{-3}
AA phosphorylation	-1.79
AA-P·IIE on-rate	0.035
AA-P·IIE off-rate	-0.034
AA dephosphorylation	see Table 2

Table 2: **Kinetic rate constants only employed in the *in vivo* simulation.** The determination of control coefficients $C_j^{RNAPol(\sigma^F)}$ is described in the main text.

rates	$C_j^{RNAPol(\sigma^F)}$	simulation value	Ref
AA dephosphorylation	3.24	3.2×10^{-3}	Fig. 5A, [32]
σ -RNAPol on-rate	0.33	10^6	[27]
σ^F -RNAPol off-rate	-0.78	0.55	[27]
σ^A -RNAPol off-rate	0.45	0.02	[27]
AB degradation	n/a	4.1×10^{-4}	[10]